Journal of Power Sources 190 (2009) 525–533

Contents lists available at ScienceDirect

Journal of Power Sources

journal homepage: www.elsevier.com/locate/jpowsour

Hydrogen production by steam reforming of ethanol over Ni-based catalysts promoted with noble metals

Luciene P.R. Profeti[a], Joelmir A.C. Dias[b], José M. Assaf[c], Elisabete M. Assaf[a,*]

[a] Universidade de São Paulo, Instituto de Química de São Carlos, CEP 13560-970, São Carlos, SP, Brazil
[b] PETROBRAS/SA-Refinaria de Paulínia, REPLAN, CEP 13140-000, Paulinia, SP, Brazil
[c] Departamento de Engenharia Química, Universidade Federal de São Carlos, C.P. 676, 13565-905 São Carlos, SP, Brazil

ARTICLE INFO

Article history:
Received 22 October 2008
Received in revised form 18 December 2008
Accepted 22 December 2008
Available online 31 December 2008

Keywords:
Nickel
Promoters
Lanthanum
Hydrogen
Ethanol
Reforming

ABSTRACT

The catalytic activity of Ni/La_2O_3-Al_2O_3 catalysts modified with noble metals (Pt and Pd) was investigated in the steam reforming of ethanol. The catalysts were characterized by ICP, S_{BET}, X-ray diffraction, temperature-programmed reduction, UV–vis diffuse reflectance spectroscopy and X-ray absorption fine structure (XANES). The results showed that the formation of inactive nickel aluminate was prevented by the presence of La_2O_3 dispersed on the alumina. The promoting effect of noble metals included a marked decrease in the reduction temperatures of NiO species interacting with the support, due to the hydrogen spillover effect, facilitating greatly the reduction of the promoted catalysts. It was seen that the addition of noble metal stabilized the Ni sites in the reduced state throughout the reaction, increasing ethanol conversion and decreasing coke formation, irrespective of the nature or loading of the noble metal.

1. Introduction

Currently, the need for renewable sources of energy is increasing, since our dependence on fossil fuels has caused serious environmental problems, namely atmospheric pollution and the greenhouse effect, and the depletion of natural resources. The use of hydrogen as a fuel could be crucial in the development of a sustainable clean energy technology, since its consumption in fuel cell devices produces only water. However, to support a feasible hydrogen-based economy, it is essential to produce hydrogen cleanly and renewably.

Among the various processes used to obtain hydrogen, the steam reforming of natural gas and methanol are the commonest, but these are nonrenewable sources, besides failing to remove the great amounts of CO_2 emitted in the reaction. From an environmental point of view, the reforming of ethanol is an interesting alternative, because this alcohol can be a renewable raw material, which can easily be derived from biomass, and the carbon dioxide produced in the reforming process is then consumed in biomass growth, thus completing a nearly closed carbon cycle. Moreover, ethanol has other advantages, such as low toxicity, storage and a handling safety, and a relatively high hydrogen content, described by reaction (1) [1]:

$$C_2H_5OH + 3H_2O \rightarrow 6H_2 + 2CO_2 \quad (1)$$

Ethanol steam reforming comprises several catalytic steps, which depend on the nature of the catalyst [2–8]. Such reaction pathways include dehydration, decomposition and dehydrogenation of ethanol to form ethylene, methane (or acetone) and acetaldehyde, respectively, besides the water-gas shift reaction (WGSR) and methanation reaction [1]. Additionally, the undesirable formation of coke can occur by the decomposition of methane, ethylene polymerization or the Boudouard reaction. Coke deposition on the catalyst surface is the main reason for the deactivation of catalysts over time, which limits their industrial application.

In a number of different studies, various metal catalysts (Ni [2], Co [3,4], Ni–Cu [5], Pt, Pd, Rh [6–8] supported on metal oxides (Al_2O_3, La_2O_3, ZnO, MgO, etc. [9]) have proved to be suitable for the ethanol steam reforming reaction. Among the transition metals, Ni has exhibited catalytic activities comparable to those of the noble metals. Its high selectivity toward hydrogen production combined with a relatively low cost makes it an appropriate active phase for practical use. However, Ni-based catalysts suffer from deactivation by coking and sintering more severely than the noble metal-based catalysts, shortening their lifetime. Nevertheless, it is possible to

* Corresponding author. Tel.: +55 16 33739951; fax: +55 16 33739952.
E-mail address: eassaf@iqsc.usp.br (E.M. Assaf).

0378-7753/$ – see front matter © 2009 Elsevier B.V. All rights reserved.
doi:10.1016/j.jpowsour.2008.12.104

counter these shortcomings by modifying the catalyst by adding metal promoters.

Several groups have reported the use of Ni-based catalysts modified by promoters for methane reforming, but their use in ethanol steam reforming is rare. In a recent study Soyal-Baltacıoglu et al. [10] investigated the ethanol reforming on catalysts having 0.2–0.3 wt.% Pt and 10–15 wt.% Ni contents. It was found that the best ethanol steam reforming performance was achieved over 0.3 wt.% Pt–15 wt.% Ni/δ-Al_2O_3. Vizcaíno et al. [11] investigated the ethanol steam reforming on Ni catalysts promoted by Mg. It was found that the addition of Mg promoter improved the catalytic performance of the nickel species and decreased the catalyst deactivation. Moreover, an important reduction in the amount of deposited coke due to inhibition of ethanol dehydration towards ethylene was observed.

The effect of the addition of cobalt on the catalytic performance of Ni catalyst in the steam reforming of ethanol was measured by Resini et al. [12]. The authors observed that the addition of Co resulted in the inhibition of the dehydration reaction as well as of methane production.

The effect of the promoters Ce, Co, Cu, Mg and Zn on the catalytic performance of Ni catalyst in the auto-thermal reforming of ethanol was investigated by Youn et al. [13]. The authors observed that the Cu was the most efficient promoter for the production of hydrogen; mainly due to the Cu species were also active in the WGSR. Furthermore, the Cu decreased the interaction between Ni-species and γ-Al_2O_3, facilitating the reduction of Ni-Cu/γ-Al_2O_3 catalyst.

It was found that the addition of small amounts of noble metals caused a significant increase in the catalytic activity of Ni for methane reforming reactions. Dias and Assaf [14–16] studied the effect of introducing small amounts of Pt, Pd and Ir into Ni/Al_2O_3 catalysts for the autothermal reforming of methane, with the aim of making the reaction ignite without previous reduction of the catalyst with H_2. It was concluded that the samples promoted with palladium nitrate were very active in the auto-thermal reforming of methane, and this was attributed to expansion of the metal surface.

On the other hand, the characteristic of the supports may influence drastically the catalytic activity of the Ni-based catalysts. This influence depends on the chemical and textural property of the support, and is related to the stability and dispersion of the metal; besides, the support participates in the reforming reaction. The selection and modification of an appropriate support for a nickel catalyst, therefore, is potentially a way to improve the catalytic performance of a supported nickel catalyst.

The support often used in reforming reactions is alumina, chosen for its mechanical and chemical resistance under reaction conditions, combined with its high surface area. However, in the case of the ethanol steam reforming reaction, the acidic sites of the γ-Al_2O_3 favor ethanol dehydration and, consequently, the formation of undesirable reaction byproducts, such as ethylene, which then undergoes polymerization to form coke [1,9]. Additionally, the use of alumina-based catalysts at high working temperatures leads to unwanted phase transitions, sintering of the active metal and the formation of an inactive metal–aluminate phase. In order to overcome these limitations, additives based on rare-earth elements are used to diminish the acid character of the γ-Al_2O_3, as well as to improve the metal dispersion and to prevent the sintering of the active metal.

Researches have described the effect produced by the addition of lanthanum as remarkable [17–20]. Martinez et al. [17] investigated the influence of lanthanum oxide added to a Ni/Al_2O_3 catalyst on the carbon dioxide reforming of methane. The authors observed that the presence of La increased the metal dispersion, increased conversion levels, and also enhanced the catalyst stability by significantly decreasing in coke formation during the reaction.

Liberatori et al. [18] investigated the catalytic behavior of Ni/Al_2O_3 catalysts modified with La and Ag in the steam reforming of ethanol. They found that the addition of La decreased the coking on Ni catalysts during the steam reforming of ethanol and promoted the selectivity to hydrogen. This resistance to coke deposition on the catalyst was attributed to the formation of lanthanum oxycarbonate, which reacts with surface carbon to form CO and regenerate La_2O_3.

Ethanol steam reforming was studied by Sánchez-Sánchez et al. [19] on alumina-supported nickel catalysts modified with Ce, Mg, Zr and La. Among these supports, the La_2O_3–Al_2O_3 showed the highest metal dispersion. The same authors also studied ethanol steam reforming on nickel catalysts supported on Al_2O_3 modified with various amounts of lanthanum [20]. The results revealed an enhancement in the stability of the Ni catalysts during reforming, with rising lanthanum loading on Al_2O_3, probably due to the enhanced ability of the nickel surface and/or La–Ni interactions to prevent the formation of carbon species.

Although several articles exist on promoted Ni/Al_2O_3 catalyst for methane reforming, the effect of adding noble metals to nickel catalysts on ethanol reforming has not been investigated in detail. Thus, the idea of the present study was to develop an alternative catalyst, based on Ni/La_2O_3-Al_2O_3 promoted with noble metals, for the ethanol steam reforming reaction, aiming at hydrogen production for fuel cell applications. These catalysts might combine the properties of nickel promoted with small amounts of noble metal in reducing the formation of CO, with the properties of the La_2O_3-Al_2O_3 support, in reducing the ethene and coke formation.

2. Experimental

2.1. Catalyst preparation

The La_2O_3-Al_2O_3 mixed oxide support was synthesized by impregnating γ-Al_2O_3 (Degussa) with $La(NO_3)_3{\cdot}6H_2O$ (Aldrich). The alumina was calcined beforehand for 5 h at 550 °C in order to stabilize the phase and eliminate surface impurities. A known amount of the nitrate precursor was dissolved in water and the γ-Al_2O_3 was added to the solution under continuous stirring. The slurry was heated to 70 °C in a rotavapor and maintained at that temperature until nearly all the water had evaporated. The solid residue was dried at 90 °C overnight and then calcined at 550 °C for 5 h under flowing air (30 cm^3 min^{-1}). The La_2O_3 content of the support was 8% by mass. The support was then impregnated with the $Ni(NO_3)_2{\cdot}6H_2O$ (Aldrich) aqueous solution, followed by the drying and calcination procedures already described. The same method was also used to add the noble metals on the Ni/La_2O_3-Al_2O_3 catalysts, using $PdCl_2$ (Aldrich) and H_2PtCl_6 (Aldrich) solutions and annealing at 600 °C. The nominal metal loading for these catalysts was 15 wt.% for Ni and 0.1 and 0.3 wt.% for Pd and Pt, respectively. The catalysts were labeled as follows: Ni/LaAl, Ni0.1Pd/LaAl, Ni0.1Pt/LaAl, Ni0.3Pd/LaAl, Ni0.3Pt/LaAl.

2.2. Catalyst characterization

The chemical composition of the catalysts was determined by inductively coupled plasma atomic emission spectroscopy (ICP–AES), using a PerkinElmer Optima 3300DV apparatus. The samples were first dissolved in acid solutions (a mixture of HF, HCl and HNO_3), and diluted to concentrations within the detection range of the instrument.

The surface areas of the catalysts were measured in a Quantachrome Nova 2.0 gas adsorption analyzer. The samples were previously outgassed at 300 °C for 2 h. N_2 adsorption–desorption isotherms were obtained at 77 K and the specific areas were calcu-

Table 1
Characterization of the catalysts.

Catalyst	Ni[a] (wt.%)	La[a] (wt.%)	M[a] (wt.%)	Ni[b] particle size (nm)	BET surface area ($m^2\ g^{-1}$)	Pore diameter (nm)	Pore volume ($cm^3\ g^{-1}$)
Al_2O_3	–			–	194	4.3	0.42
La_2O_3-Al_2O_3	–			–	129	3.9	0.25
Ni	12.6	9.0	–	13	114	4.5	0.26
Ni0.1Pd	12.4	6.4	0.13	24	132	4.4	0.29
Ni0.3Pd	12.7	6.9	0. 33	26	133	4.2	0.27
Ni0.1Pt	12.1	6.4	0.04	17	139	4.5	0.26
Ni0.3Pt	11.6	6.3	0.23	19	138	4.4	0.29

[a] Determined by ICP.
[b] Determined by XRD.

lated from these isotherms using the Brunauer–Emett–Teller (BET) method.

The crystalline structures of the catalysts were investigated by X-ray diffraction (XRD) performed on a Rigaku Multiflex diffractometer using a CuK_α radiation source. The X-ray diffractograms were collected for 2θ values ranging from 10° to 80°. The apparent size of nickel oxide particles was calculated by the Scherrer's formula, $L = 0.9\lambda/\beta_{2\theta}\cos\theta_{max}$, where λ is the X-ray wavelength (1.54056 Å for the CuK_α radiation), $\beta_{2\theta}$ is the width of the NiO diffraction peak at half-height, and θ_{max} is the Bragg angle at the peak maximum position.

UV–vis diffuse reflectance spectroscopy (DRS) was carried out in a Varian Cary 5G UV–vis/NIR spectrophotometer equipped with a diffuse reflectance accessory in the range of 200–800 nm. The Kubelka–Munk function $F(R)$ was calculated using barium sulphate as the reference material.

The incorporation of the noble metals on the nickel catalysts was investigated by thermogravimetric analysis (TGA) and differential thermal analysis (DTA), which were performed in a Mettler Toledo (TGA/SDTA851e) thermobalance. A sample of 20 mg was heated at 10 °C min^{-1} to 1000 °C under flowing air (100 $cm^3\ min^{-1}$). The positive peaks in the TGA curves are related to the exothermic process.

Temperature-programmed reduction (TPR) experiments were performed with 25 mg catalyst in a quartz U-shaped tube reactor in a Micromeritics Pulse Chemisorb 2705, subjected to a temperature ramp from 35 to 1000 °C at 10 °C min^{-1}. The sample was reduced with 2% H_2 in argon, flowing at 30 $cm^3\ min^{-1}$. A thermal conductivity detector (TCD) was employed to determine the amount of hydrogen consumed.

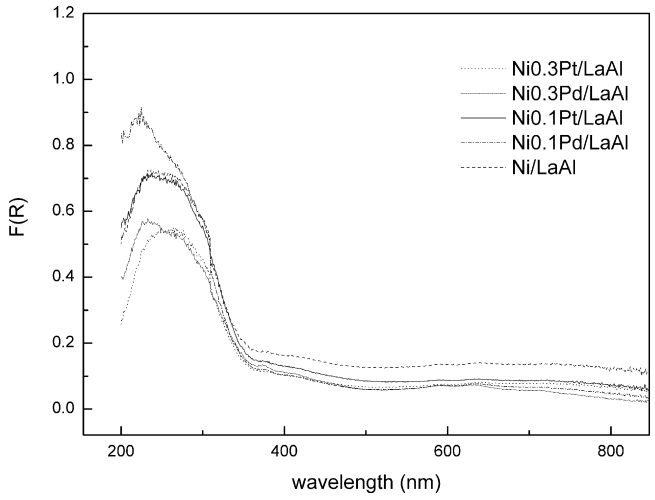

Fig. 1. UV–vis spectra of the promoted and unpromoted Ni/LaAl catalysts and La_2O_3-Al_2O_3 support.

In situ H_2-TPR/X-ray absorption fine structure (XANES) studies were performed by dispersive-geometry X-ray absorption spectroscopy at D06A-DXAS beam-line of the Laboratório Nacional Luz Síncrotron (LNLS). A Si(1 1 1) monochromator was used to select the energy, and the beam was focused at the sample position. The experimental setup has been described in more detail by Meneses et al. [21] and consists of a compact furnace with halogen lamps as heater elements and a quartz tube sample chamber with ends closed with aluminium flanges sealed by Kapton windows. The catalyst sample was fixed in a stainless steel holder placed in the center of the quartz tube, and positioned relatively to the beam by fine adjustment of the position of the table. The reactor was purged with He for more than 30 min at 30 $cm^3\ min^{-1}$, then the reactant gas (H_2/N_2, 5%) flowed through the samples (30 $cm^3\ min^{-1}$) and a temperature ramp of 10 °C min^{-1} was applied by the furnace.

The Ni K-edge spectra were recorded in transmission mode and collected in the CCD detector with 15 ms of time exposure and 50 accumulations for each edge. A Ni foil spectrum was measured for energy calibration. The spectra for each sample were collected in the photon energy range from 8200 to 8550 eV.

2.3. Catalytic tests

The reforming reaction was conducted in a fixed-bed reactor of a quartz tube with inner diameter 13 mm at atmospheric pressure. A thermocouple was located inside the reactor tube, near of the catalyst bed. Prior to the catalytic reaction, the 150 mg of catalyst was reduced at 700 °C with H_2 flowing at 30 $cm^3\ min^{-1}$ for 1 h. After this activation of the catalyst, the ethanol and water (1:4) mixture was pumped into the reactor at a flow rate of 2.5 $cm^3\ h^{-1}$. Before entering the reactor, the mixture was preheated at 180 °C.

Condensable products (ethanol, acetaldehyde, water, acetone, etc.) were trapped at +0.5 °C at the reactor outlet and further analyzed by gas chromatography (Hewlett Packard 5890) with a flame ionic detector (FID) and a capillary column HP-FFAP. Gas was periodically sampled and analyzed with an in-line gas chromatograph (Varian, model 3800) equipped with two TCDs, a 13X molecular sieve packed (H_2 analyses) and Porapak-N columns (CO_2, CO and CH_4 analysis). The product distribution was monitored for 6 h of reaction. Catalytic activity was evaluated in terms of ethanol conversion, and the products yields are expressed as the ratios of the moles of product to the moles of ethanol supplied. The percent distribution of the gaseous products was also calculated as follows:

$$D(\%) = \left(\frac{M_P}{M_{\Sigma P}}\right) \times 100 \quad (4)$$

where M_P is the number of moles of each product, and $M_{\Sigma P}$ is the sum of the number of moles of all gaseous products.

The mass of coke deposited was measured by weighing the reactor containing the catalyst before and after the reaction and calculating the gain in mass.

3. Results and discussion

3.1. Characterization

The chemical composition and the textural properties (surface area, pore volume, average pore diameter) of the supports and the catalysts are listed in Table 1. As can be seen, the surface area and the pore volume of Al_2O_3 were reduced after the incorporation of La_2O_3, indicating introduction of La_2O_3 particles into the pores of Al_2O_3. In the unpromoted catalysts, deposition of Ni on La_2O_3-Al_2O_3 caused a slight decrease in the specific surface, which dropped from 129 to 114 $m^2\,g^{-1}$. However, the surface area of the nickel catalyst increased after the deposition of the noble metal, whereas the pore volume remains unaltered, indicating that the metal promoters combined with the nickel particles contributed to the specific surface area.

The chemical compositions of the catalysts, measured by ICP, showed general agreement between the theoretical and experimental compositions, indicating that the experimental method was appropriate for the synthesis of the catalysts.

In order to confirm the identity of nickel species, DRS was used to study the symmetry and coordination of the surface species of the catalysts. Results for the catalysts and the support are shown in Fig. 1, where the Kubelka–Munk functions of the corresponding bands are plotted as a function of the wavelength. The DRS profiles showed an intense signal in the region between 205 and 375 nm, which may be related to the NiO charge-transfer band [13]. According to the literature, these absorption bands are usually ascribed to charge transfer of octahedral Ni^{2+} species in NiO lattices [22].

It is known that the high-temperature treatment leads to the dispersion of NiO particles and an inactive $NiAl_2O_4$ phase can be formed, which is highly undesirable due to the low reducibility of nickel in aluminate compounds. Thus, the DRS measurements can be a very useful way of checking the interaction between nickel and alumina support, since the $NiAl_2O_4$ spectrum differs considerably from that of NiO. The nickel aluminate can be described as a partial inverse spinel, where the Ni(II) ions occupy both octahedral and tetrahedral sites in the oxygen lattice, and show characteristic absorption bands in the range 600–645 nm [23,24].

As can be seen, in the present results (Fig. 1) no peaks assigned to nickel aluminate species were found, either for the promoted or the unpromoted nickel catalysts. These results agree with the TPR results (see below), where no reduction peak at high temperature (above 800 °C) assigned to nickel aluminate was observed.

The crystalline phases present in the Ni/LaAl and NiM/LaAl catalysts investigated by X-ray diffraction analysis. The XRD patterns of these catalysts are presented in Fig. 2. All samples showed diffraction lines characteristic of the poorly crystalline γ-Al_2O_3 support (at ∼37°, 46° and 67° – JCPDS 46-1131), but no peaks attributed to the La_2O_3 phases were detected. A similar behavior has been observed elsewhere with La_2O_3-Al_2O_3 supported catalysts, where only diffractions peaks corresponding to alumina phases are obtained [25,26].

The presence of NiO was confirmed by the diffraction peaks located at $2\theta = 43.3°$, 63.7° and 75.5° (JCPDS 44-1159). The broadened NiO peaks observed for all samples suggest that the sample is not highly crystallized, as well as being due to either the formation of well-dispersed Ni species or the existence of small NiO particles. Similar XRD patterns were obtained for the promoted catalysts, indicating that no new phase was formed by the incorporation of the noble metals.

In the diffractograms it is difficult to identify the formation of $NiAl_2O_4$, since in the broadened XRD patterns, the signals from nickel spinel and γ-$A1_2O_3$, having very similar crystal lattices, overlap. The average crystal particle size was calculated from X-ray diffractograms by the Scherrer's equation using the NiO diffraction peak at $2\theta = 43.3°$. Table 1 show that values vary between 13 nm for Ni/LaAl and 17–26 nm for the promoted catalysts. Hence, the second thermal treatment for the incorporation of noble metal provoked crystallization and crystal growth, thus enlarging the particles.

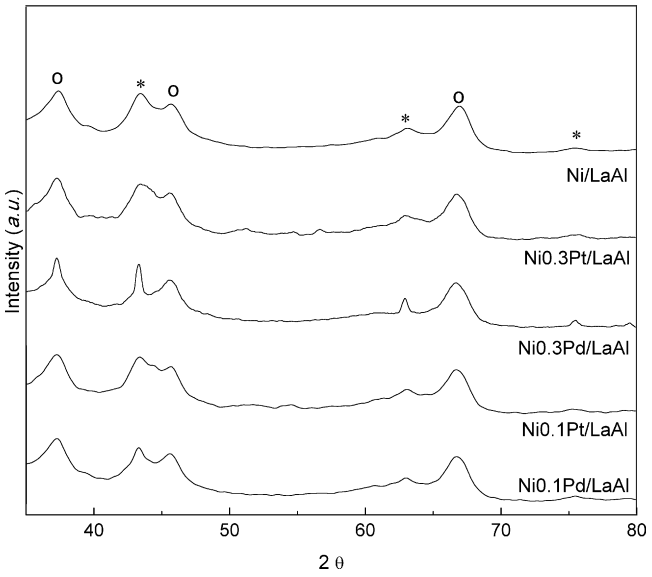

Fig. 2. X-ray diffractograms of the unpromoted and promoted Ni/LaAl catalysts.

The TGA and DTA analyses were performed in order to determine the Pt and Pd species formed during calcinations. Fig. 3a shows the TGA and DTA analyses of the calcined Ni/LaAl catalyst, where only a small weight loss occurred between 400 and 800 °C, probably due to the elimination of some adsorbed water and further crystallization of the NiO particles.

The thermogravimetric analyses of the promoted catalysts were performed soon after the impregnation of the Pt and Pd precursors. Fig. 3b and c shows the TGA–DTA of Ni0.1Pt/LaAl and Ni0.3Pt/LaAl, respectively. Three decomposition stages were observed, which take place in the temperature range 200–800 °C. According to Radivojević et al. [27], these three steps are related to the decomposition of the Pt precursor ($H_2PtCl_6{\cdot}6H_2O$) in oxidizing atmosphere following the reactions:

$$H_2PtCl_6{\cdot}6H_2O \rightarrow PtCl_4 + 2HCl + 6H_2O \quad (2)$$

$$PtCl_4 \rightarrow PtCl_2 + Cl_2 \quad (3)$$

$$PtCl_2 \rightarrow Pt + Cl_2 \quad (4)$$

Simultaneously recorded DTA curves show that all these losses correspond to exothermic peaks. Additionally, PtO_x species may be formed at higher temperatures under air flow and may also be accompanied by some crystallization, resulting in exothermic processes [27].

Fig. 3d and e shows the TGA–DTA curves of Ni0.1Pd/LaAl and Ni0.3Pd/LaAl, respectively. Two stages of weight loss occurred from 200 to 450 °C, which correspond to exothermic peaks. This loss is probably related to the thermal decomposition of $PdCl_2$, in analogous processes to these described for the platinum precursors, and the formation of an oxide phase (PdO) [28]. After these results were obtained, the calcination process for noble metal incorporation was performed at 600 °C.

Fig. 4 shows the TPR profiles of supported Ni catalysts. The reduction pattern of the Ni/LaAl catalyst may be divided into four regions. According to published studies, the peak temperature for pure NiO reduction is about 325 °C [17]. Hence, the low temperature reduction peak at around 400 °C can be assigned to the reduction of

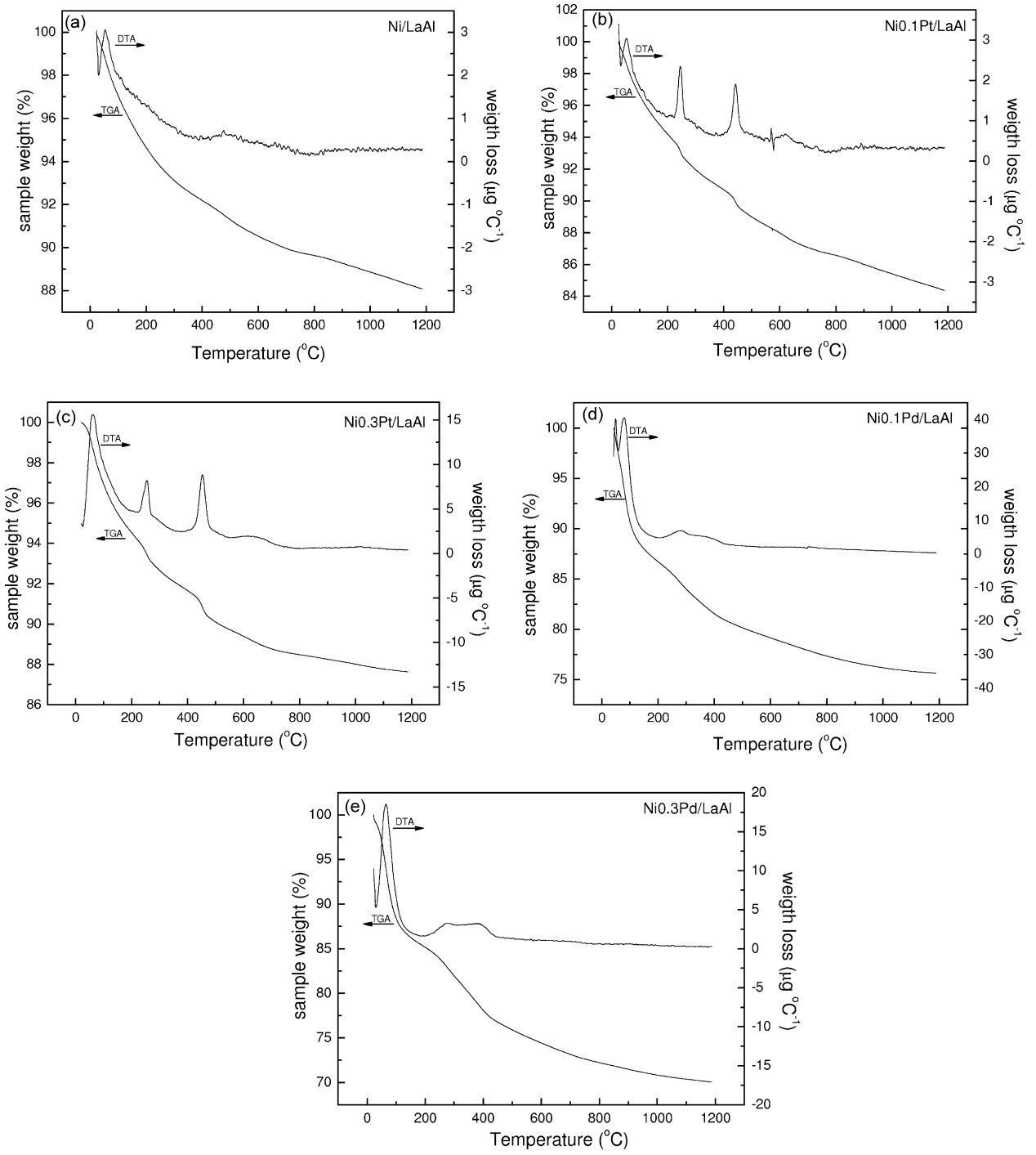

Fig. 3. TGA–DTA curves of NiM/LaAl, under air flow at 10 °C min^{-1} after the impregnation of the noble metals precursor solutions.

NiO species interacting weakly with the alumina support [29]. The broad high-temperature reduction peaks above 500 °C could be due to the reduction of a well-dispersed and possibly amorphous NiO phase that interacts strongly with the support [17]. Moreover, it is known that the addition of lanthanum to Al_2O_3 by the impregnation method can hinder the reduction of the NiO, owing to an increase in the proportion of highly dispersed nickel species (peak at ~630 °C) and a concomitant decrease in the proportion of nickel with interacting weakly with the support (peak at ~540 °C), compared to those catalysts prepared without lanthanum. This increase in the reduction temperature is related to the presence of nickel in a surface phase containing Ni, Al, and La, in which nickel interaction is higher [17]. Additionally, the peak at ~880 °C may be attributed to the reduction of a stable nickel species [14].

In the catalysts promoted with Pd, three well-defined regions of NiO reduction were observed. The initial reduction temperature was decreased slightly from 465 °C (Ni/LaAl) to about 418 °C and the area of this reduction peak was increased, whereas the area of the peaks located at higher temperatures was decreased. These results indicate that the amount of reducible Ni species was increased, and the addition of the Pd facilitated the reduction of the species interacting strongly with the support. Furthermore, the amount of Pd added also influenced the degree of reduction, as can be observed by comparing the increase in the area related to the first reduction

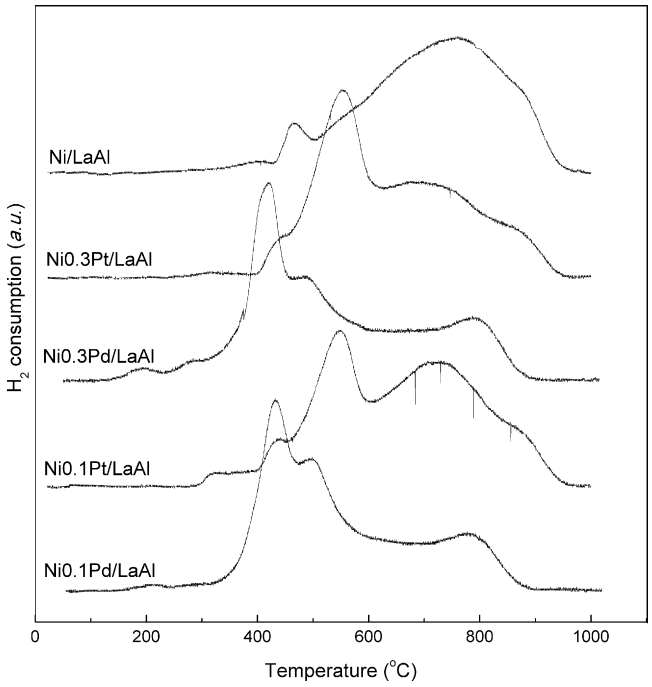

Fig. 4. TPR profiles of the promoted and unpromoted Ni/LaAl catalysts.

process (at 418 °C) for the Ni0.3Pd/LaAl with that of Ni0.1Pd/LaAl. The reduction profiles of the Pt-promoted catalysts showed four well-defined regions of NiO reduction, and the area of the second peak increased significantly.

The decrease of the temperature of the NiO reduction, seen in the TPR curves of the promoted catalysts, may result from a hydrogen spillover phenomenon that occurs in noble metals [30–32]. On the promoted catalysts, the hydrogen is first dissociated on the reduced noble metal clusters, forming active hydrogen, which can migrate and reduce the neighboring nickel oxide clusters. These results indicate that the presence of noble metal facilitates the reduction of nickel species.

This behavior may be confirmed by the TPR-XANES analysis, where we can follow the trajectory of the chemical reactions occurring during the reduction experiment. In this case, the pre-edge peak intensity and white line intensity are considered the main characteristics for monitoring the reduction of the nickel species. The Ni K-edge XANES spectra for Ni/LaAl catalysts monitored during the reduction process are shown in Fig. 5. For all samples, the first spectrum at room temperature resembles that of NiO (Fig. 6), with a high intensity of the white line, caused by the Ni–O interaction [33]. The appearing of a pre-edge is also observed, which is due to the forbidden dipole and allowed quadrupole transitions from the Ni 1s orbitals to Ni 3d orbital [34]. As the temperature is increased under reducing conditions, the intensity of the white line decreases and the spectra assume a similar profile to the Ni foil spectrum (Fig. 6), showing that Ni^{2+} is converted to Ni^0. Fig. 5a shows that the reduction of the Ni/LaAl catalyst begins at 550 °C, where a slightly decrease in the intensity of the white line is observed. A shift of the absorption edge energy towards lower values is also observed in the course of the reaction, as it assumes the photon energy values characteristic of metallic Ni [33].

The addition of the noble metals to the Ni catalyst caused a marked modification of the Ni K-edge XANES spectra from 400 °C, corroborating the TPR results for the promoted samples. Fig. 5b shows the evolution of the reduction reaction of the Ni0.3Pd/LaAl catalyst and the white line intensity is seen to drop from 350 °C, followed by the shift in the absorption edge, whereas the Ni/LaAl

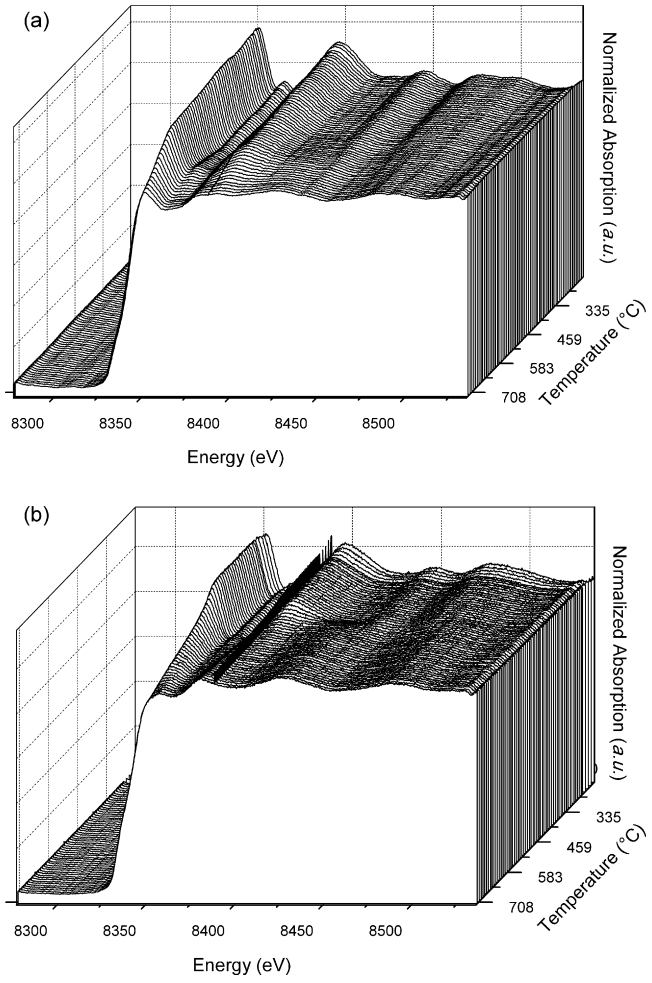

Fig. 5. *In situ* TPR-XANES spectra of Ni/LaAl (a) and Ni0.3Pd/LaAl (b) catalysts under reduction conditions from 25 up to 800 °C.

catalyst was reduced at higher temperatures. The spectra of the other promoted catalysts are similar to that of the Ni0.3Pd/LaAl catalyst and not shown for the sake of brevity. Therefore, in Fig. 7 the variation of the white line intensity with rising temperature is shown for all samples and it is clear that the noble metals catalyze

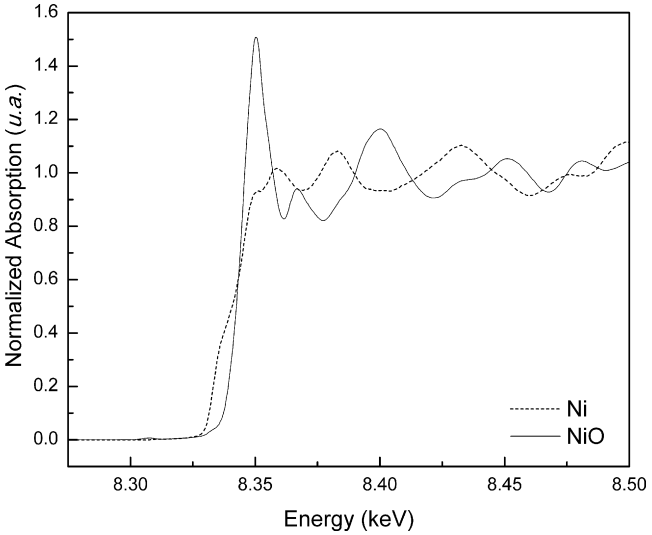

Fig. 6. Ni K-edge XANES spectra of (a) NiO and (b) Ni foil.

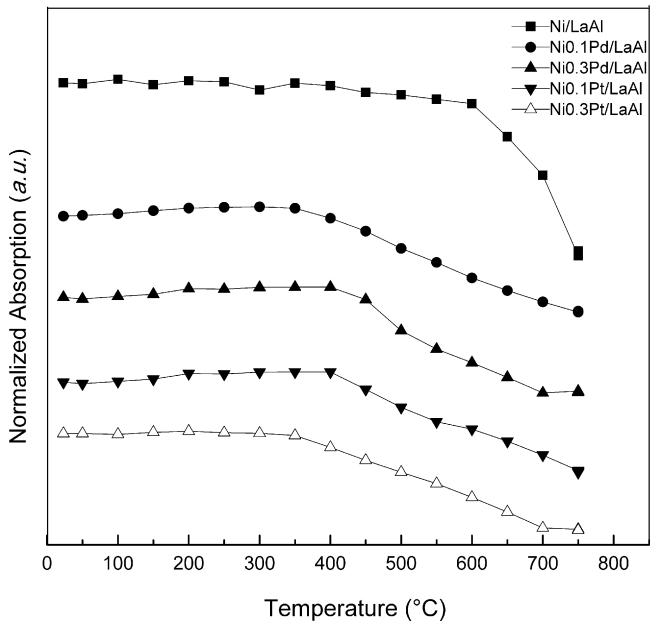

Fig. 7. White line intensities as a function of temperature for unpromoted and promoted Ni/LaAl catalysts.

the reduction of the nickel species. This enhancement of reducibility may be closely related to the improved catalytic performances of the promoted catalysts, as seen below.

3.2. Catalytic tests

The catalytic activity of the Ni/LaAl catalysts for the ethanol steam-reforming reaction was studied between 450 and 600 °C at atmospheric pressure. From the analysis of the exit gases, it appears that hydrogen is the main component of the reaction products, which also include CO, CO_2 and CH_4. Some acetaldehyde was detected in the analyses of the condensable products. No ethylene was formed at any temperature investigated, indicating that the addition of lanthanum to the alumina suppressed the acid sites required for the dehydration of the ethanol.

The gaseous product distribution obtained at 600 °C, especially with regard to the amounts of CO, CO_2 and CH_4 produced, is very similar for all catalysts: 60–70% H_2, 15–20% CO_2, 9–12% CO and 9–12% CH_4, as shown in Fig. 8. This hydrogen yield is close to the value observed by Sánchez-Sánchez et al. [19] in nickel catalysts dispersed on La_2O_3-Al_2O_3 supports.

Regarding the mechanism of ethanol steam reforming, besides reaction (1), other reactions may occur, taking account of the formation of H_2, CO_2, CO, CH_4, and CH_3CHO, by partial ethanol decomposition (reaction (5)), ethanol dehydrogenation to acetaldehyde (reaction (6)) and the WGSR (reaction (7)) [1]:

$$C_2H_5OH \rightarrow CH_4 + CO + H_2 \quad (5)$$

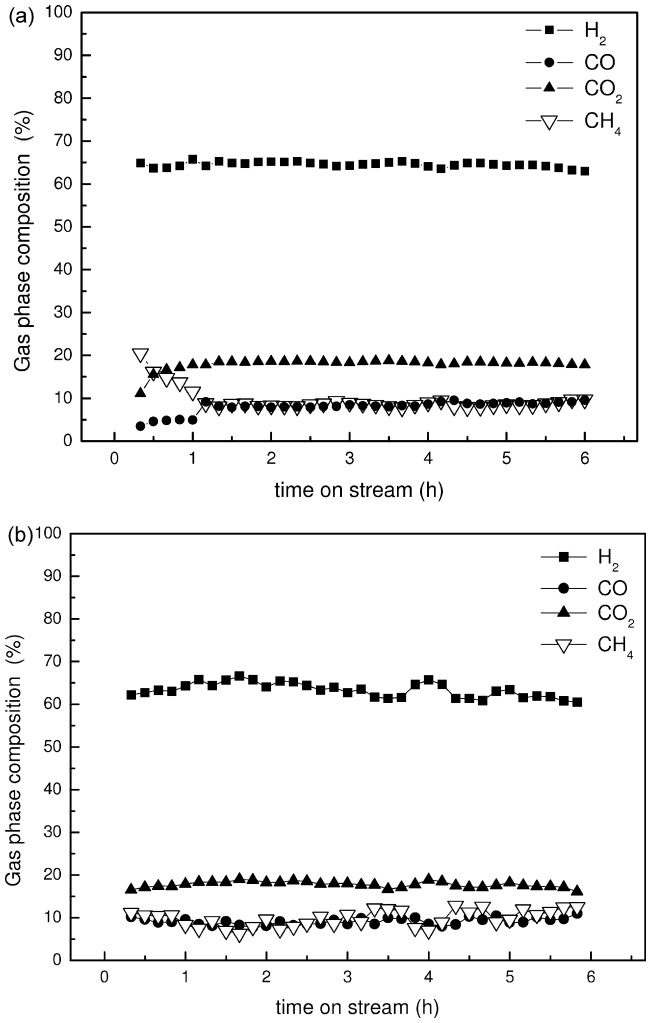

Fig. 8. Formation of gaseous products for the (a) Ni/LaAl and (b) Ni0.1Pt/LaAl catalysts at 600 °C.

$$C_2H_5OH \rightarrow CH_3CHO + H_2 \quad (6)$$

$$CO + H_2O \rightleftharpoons H_2 + CO_2 \quad (7)$$

Tables 2 and 3, respectively, compare the average number of moles of products formed per mole of ethanol supplied and the ethanol conversion, at 450 and 600 °C. As can be observed, the ethanol–steam reaction performed at 450 and 600 °C showed similar ethanol conversion values, higher values being obtained with the promoted catalysts, irrespective of the noble metal loading. As expected, the production of H_2 and CO increased with the increase in temperature, whereas the formation of CO_2 and CH_4 diminished. The CO enrichment in the gas effluent at higher temperatures may be explained by the reverse WGSR (7), which takes place simultaneously in the reactor. The WGSR is exothermic and the equilibrium

Table 2
Average product yields (*Y*) of ethanol steam reforming of unpromoted and promoted Ni/LaAl catalysts (mol produced/mol ethanol supplied).

Catalyst	YH_2		YCO		YCO_2		YCH_4		YCH_3CHO*	
	450 °C	600 °C	450 °C	600 °C	450 °C	600 °C	450 °C	600 °C	450 °C	600 °C
Ni	1.76	3.44	0.09	0.43	0.93	0.98	1.23	0.52	105.76	0.97
Ni0.1Pd	2.27	3.78	0.08	0.55	1.23	0.97	1.48	0.52	0.66	1.44
Ni0.3Pd	2.23	3.71	0.10	0.47	1.19	0.93	1.38	0.59	0.44	2.90
Ni0.1Pt	2.52	3.79	0.11	0.53	1.41	1.03	1.71	0.62	0.40	0.36
Ni0.3Pt	2.25	3.80	0.08	0.55	1.25	1.05	1.55	0.51	0.76	7.86

* mmol CH_3CHO/mol ethanol supplied.

Table 3
Conversion values of ethanol (*C*) and coke formed during ethanol steam reforming for unpromoted and promoted Ni/LaAl catalysts.

Catalyst	C (%)		Coke (mmol h^{-1})	
	450 °C	600 °C	450 °C	600 °C
Ni	67	86	1.32	0.69
Ni0.1Pd	99	99	0.86	0.23
Ni0.3Pd	99	96	0.64	0.27
Ni0.1Pt	99	96	0.69	0.43
Ni0.3Pt	97	94	0.78	0.41

shifts to the left at higher temperatures, favoring the formation of CO. This interpretation supported by the higher CO_2 formation at 450 °C, where the WGSR favored H_2 and CO_2 production.

The decrease in the formation of methane at higher temperatures may be justified by its production being thermodynamically favored at low temperatures, so that the formation of CH_4 declines rapidly above 500 °C [7]. Additionally, it has been proposed that methane is also formed by methanation of CO (reaction (8)), which is thermodynamically favored at temperatures below 530 °C:

$$CO + 3H_2 \rightarrow CH_4 + H_2O \quad (8)$$

The presence of CH_4 in the reaction products is undesirable because its production by reaction (5) diminishes the hydrogen yield, compared to reaction (1), and methanation would actually consume H_2 [1].

It was expected that the noble metals could cause a decrease in the concentrations of CO in the product stream. However, this promotion effect was not observed. In fact, the CO formation was somewhat higher in the promoted catalysts than in the unpromoted one, probably due to the low catalytic activity for the WGSR found in the Ni catalysts [9], which was not improved by the addition of noble metal.

The incorporation of the noble metals in Ni/LaAl catalysts caused only slight differences in the distribution of gaseous products. On the other hand, the effect of the noble metal on catalytic performance is clearly observed in the ethanol conversion values, which are higher for the promoted catalysts, as observed in Table 3. The H_2 yield was also enhanced for the promoted catalysts at both 450 and 600 °C. More importantly, the production of undesirable byproducts at 450 °C, such as acetaldehyde, was significantly suppressed on incorporation of the noble metal (Table 2).

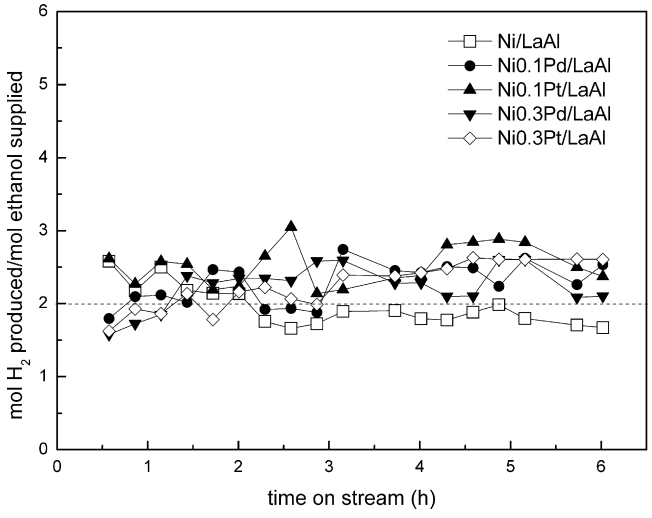

Fig. 9. H_2 yields obtained for the promoted and unpromoted Ni/LaAl catalysts at 450 °C.

Fig. 9 shows the moles of H_2 produced per mole of ethanol supplied at 450 °C, and it is observed that at the beginning, the H_2 production on the Ni/LaAl catalyst is about 2.5 mol per mole ethanol, but this decreases progressively to ~1.8 mol after 2 h, remaining approximately constant until the end of experiment (~1.6 mol). This behavior indicates that the nickel species undergoes a small deactivation process during the reaction. However, this phenomenon was not observed in the promoted catalysts up to 6 h of reaction. Liberatori et al. [18] found that the Ni in La-containing catalysts (15Ni/12La–Al_2O_3) is highly susceptible to oxidation by water at low temperatures, and the Ni in oxide form is inactive for ethanol steam reforming at low temperature. Thus, it appears that the addition of small amounts of noble metal probably prevents the reoxidation of Ni sites, becoming the Ni/LaAl catalyst less susceptible to the deactivation during the reforming reaction. This beneficial effect is observed for all the promoted catalysts, irrespective of the nature or loading of the noble metal.

The slight fall in the H_2 production on the Ni/LaAl catalyst may also be attributed to carbon deposition on the surface. Table 3 indicates the rate of the carbon formation (mmol h^{-1}) for all catalysts, measured by the amount of coke recovered at the end of each reaction. It is evident that another effect of the noble metal is a considerable decrease in coke formation on the promoted catalysts at both temperatures studied (Table 3). The coke may be formed by decomposition of CH_4 (reaction (9)), polymerization of C_2H_4 or Boudouard reaction (reaction (10)) [1]:

$$CH_4 \rightarrow 2H_2 + C \quad (9)$$

$$CO_2 \rightarrow O_2 + C \quad (10)$$

In the case of these catalysts, the production of ethylene was clearly inhibited on La_2O_3-Al_2O_3-supported catalysts, since it was not found as a by-product. Thus, these results suggest that carbonaceous species were probably formed by methane decomposition or the Boudouard reaction, which occur less extensively on the promoted catalysts.

Although some coke accumulated in the reactor over time, the product composition remained relatively constant throughout the reaction for the promoted catalysts, confirming that the contribution of these small amounts of noble metals on the Ni/LaAl catalysts is not only to increase the performance, but also stabilize the metallic state of Ni and thus preserve the catalytic activity.

In summary, for ethanol steam reforming at 450 and 600 °C, the promoted catalysts showed higher H_2 production and higher ethanol conversion. These results demonstrated that the supported-Ni promoted catalysts are suitable materials for hydrogen production by ethanol steam reforming, but that CO selectivity must be reduced for fuel cell applications. Further studies related to the minimizing of CO formation are in progress.

4. Conclusions

NiM/LaAl (M = Pd, Pt) catalysts with two different noble metal contents (0.1 and 0.3 wt.%) were prepared by the impregnation method and applied to hydrogen production by ethanol steam reforming. The effects on the properties and catalytic activity of the NiM/LaAl were investigated. Results of TPR and TPR-XANES analyses showed that significant changes occur in the oxidation states of Ni due to the addition of noble metals. The addition of small amounts of the promoter metals caused a decrease in the reduction temperature of NiO, owing to a hydrogen spillover effect.

Experimental tests of ethanol steam reforming showed that the Ni/LaAl promoted catalysts produced a hydrogen-rich gas mixture. In the experiments performed at 450 °C, the Ni/LaAl catalyst showed lower H_2 formation and higher acetaldehyde production than the promoted catalysts. Moreover, the bimetallic catalysts

showed a higher ethanol conversion and higher hydrogen yield than the Ni/LaAl catalyst, irrespective of the nature or concentration of the noble metal.

Acknowledgements

The authors thank FAPESP and CNPq for financial assistance, the Brazilian Synchrotron Laboratory (LNLS) for the XANES experiments and DEQ/UFSCar for BET and XRD analyses.

References

[1] A. Haryanto, S. Fernando, N. Murali, S. Adhikari, Energy Fuels 19 (2005) 2098–2106.
[2] J.D.A. Bellido, E.M. Assaf, J. Power Sources 177 (2008) 24–32.
[3] S. Tuti, F. Pepe, Catal. Lett. 122 (2008) 196–203.
[4] L.P.R. Profeti, E.A. Ticianelli, E.M. Assaf, J. Power Sources 175 (2008) 482–489.
[5] A.J. Vizcaíno, A. Carriero, J.A. Calles, Int. J. Hydrogen Energy 32 (2007) 1450–1461.
[6] A.C.W. Koh, W.K. Leong, L. Chen, T.P. Ang, J. Lin, B.F.G. Johnson, T. Khimyak, Catal. Commun. 9 (2008) 170–175.
[7] D.K. Liguras, D. Kondarides, X.E. Verykios, Appl. Catal. B 43 (2003) 345–354.
[8] T. Montini, L. De Rogatis, V. Gombac, P. Fornasiero, M. Graziani, Appl. Catal. B 71 (2007) 125–130.
[9] M. Ni, D.Y.C. Leung, M.K.H. Leung, Int. J. Hydrogen Energy 32 (2007) 3238–3247.
[10] F. Soyal-Baltacıoglu, A.E. Aksoylu, Z.I. Onsan, Catal. Today 138 (2008) 183–186.
[11] A.J. Vizcaíno, P. Arena, G. Baronetti, A. Carrero, J.A. Calles, M.A. Laborde, N. Amadeo, Int. J. Hydrogen Energy 33 (2008) 3489–3492.
[12] C. Resini, M.C.H. Delgado, S. Presto, L.J. Alemany, P. Riani, R. Marazza, G. Ramis, G. Busca, Int. J. Hydrogen Energy 33 (2008) 3728–3735.
[13] M.H. Youn, J.G. Seo, P. Kim, J.J. Kim, H.-I. Lee, I.K. Song, J. Power Sources 162 (2006) 1270–1274.
[14] J.A.C. Dias, J.M. Assaf, Appl. Catal. A 334 (2008) 243–250.
[15] J.A.C. Dias, J.M. Assaf, J. Power Sources 139 (2005) 176–181.
[16] J.A.C. Dias, J.M. Assaf, J. Power Sources 130 (2004) 106–110.
[17] R. Martínez, E. Romero, C. Guimon, R. Bilbao, Appl. Catal. A 274 (2004) 139–149.
[18] J.W.C. Liberatori, R.U. Ribeiro, D. Zanchet, F.B. Noronha, J.M.C. Bueno, Appl. Catal. A 327 (2007) 197–204.
[19] M.C. Sánchez-Sánchez, R.M. Navarro, J.L.G. Fierro, Int. J. Hydrogen Energy 32 (2007) 1462–1471.
[20] M.C. Sánchez-Sánchez, R.M. Navarro, J.L.G. Fierro, Catal. Today 129 (2007) 336–345.
[21] C.T. Meneses, W.H. Flores, A.P. Sotero, E. Tamura, F. Garcia, J.M. Sasaki, J. Synchrotron. Rad. 13 (2006) 468–470.
[22] J. Escobar, J.A. De Los Reyes, T. Viveros, Appl. Catal. A 253 (2003) 151–163.
[23] E. Heracleous, A.F. Lee, K. Wilson, A.A. Lemonidou, J. Catal. 231 (2005) 159–171.
[24] P. Kim, Y. Kim, C. Kim, H. Kim, Y. Park, J.H. Lee, I.K. Song, J. Yi, Catal. Lett. 89 (2003) 185–192.
[25] R.M. Navarro, M.C. Álvarez-Galván, F. Rosa, J.L.G. Fierro, Appl. Catal. A 97 (2006) 60–72.
[26] O.V. Mokhnachuk, S.O. Soloviev, A. Yu Kapran, Catal. Today 119 (2007) 145–151.
[27] D. Radivojević, K. Seshan, L. Lefferts, Appl. Catal. A 301 (2006) 51–58.
[28] M.R. Othman, I.S. Sahadan, Microporous Mesoporous Mater. 91 (2006) 145–150.
[29] J.T. Richardson, M.V. Twigg, Appl. Catal. A 167 (1998) 57–64.
[30] D. Xu, W. Li, H. Duan, Q. Ge, H. Xu, Catal. Lett. 102 (2005) 229–235.
[31] T.K. Das, G. Jacobs, P.M. Patterson, W.A. Conner, J.L. Li, B.H. Davis, Fuel 82 (2003) 805–815.
[32] G. Jacobs, T.K. Das, P.M. Patterson, J.L. Li, L. Sanchez, B.H. Davis, Appl. Catal. A 247 (2003) 335–343.
[33] W. Wen, J.E. Calderon, J.L. Brito, N. Marinkovic, J.C. Hanson, J.A. Rodriguez, J. Phys. Chem. C 112 (2008) 2121–2128.
[34] E.C. Souza, E.A. Ticianelli, Int. J. Hydrogen Energy 32 (2007) 4917–4924.